J Mater Sci (2006) 41:7704–7719
DOI 10.1007/s10853-006-0472-2

In situ TEM nanoindentation and dislocation-grain boundary interactions: a tribute to David Brandon

Jeff T. M. De Hosson · Wouter A. Soer · Andrew M. Minor · Zhiwei Shan · Eric A. Stach · S. A. Syed Asif · Oden L. Warren

Received: 29 March 2006 / Accepted: 25 May 2006 / Published online: 2 November 2006

Abstract As a tribute to the scientific work of Professor David Brandon, this paper delineates the possibilities of utilizing in situ transmission electron microscopy to unravel dislocation-grain boundary interactions. In particular, we have focused on the deformation characteristics of Al–Mg films. To this end, in situ nanoindentation experiments have been conducted in TEM on ultrafine-grained Al and Al–Mg films with varying Mg contents. The observed propagation of dislocations is markedly different between Al and Al–Mg films, i.e. the presence of solute Mg results in solute drag, evidenced by a jerky-type dislocation motion with a mean jump distance that compares well to earlier theoretical and experimental results. It is proposed that this solute drag accounts for the difference between the load-controlled indentation responses of Al and Al–Mg alloys. In contrast to Al–Mg alloys, several yield excursions are observed during initial indentation of pure Al, which are commonly attributed to the collective motion of dislocations nucleated under the indenter. Displacement-controlled indentation does not result in a qualitative difference between Al and Al–Mg, which can be explained by the specific feedback characteristics providing a more sensitive detection of plastic instabilities and allowing the natural process of load relaxation to occur. The in situ indentation measurements confirm grain boundary motion as an important deformation mechanism in ultrafine-grained Al when it is subjected to a highly inhomogeneous stress field as produced by a Berkovich indenter. It is found that solute Mg effectively pins high-angle grain boundaries during such deformation. The mobility of low-angle boundaries is not affected by the presence of Mg.

Special title: Advanced Materials and Characterization: Proceedings of the Brandon Symposium; Guest Editors: Wayne D. Kaplan and Srinivasa Ranganathan

J. T. M. De Hosson (✉) · W. A. Soer
Department of Applied Physics, Materials Science Centre and the Netherlands Institute for Metals Research, University of Groningen, Nijenborgh 4, Groningen 9747 AG, the Netherlands
e-mail: j.t.m.de.hosson@rug.nl

A. M. Minor · Z. Shan
National Center for Electron Microscopy, Lawrence Berkeley National Laboratory, One Cyclotron Road, MS 72, Berkeley, CA 94720, USA

E. A. Stach
School of Materials Engineering, Purdue University, West Lafayette, IN 47906, USA

S. A. Syed Asif · O. L. Warren
Hysitron, Inc., 10025 Valley View Road, Minneapolis, MN 55344, USA

Introduction

Microscopy in the field of materials science is generally devoted to linking microstructural observations to properties [1]. However, the actual linkage between the microstructure studied by microscopy on one hand and the physical property of a material on the other hand is almost elusive. The reason is that various physical properties are determined by the collective behavior of defects rather than by the behavior of a single defect. For instance, there exists a vast amount of electron microscopy analyses concerned with post mortem observation of ex-situ deformed materials, which try to link observed patterns of defects to the

mechanical property. However, in spite of the enormous effort that has been put in both theoretical and experimental work, a clear physical picture that can predict even one simple stress-strain curve based on these microscopy observations is still lacking.

There are at least two reasons that hamper a straightforward correlation between microscopic structural information and materials properties: one fundamental and one practical reason. Of course it has been realized for a long time that in the field of dislocations, disclinations and interfaces in materials, we are facing non-equilibrium effects. The defects determining mechanical performance are in fact not in thermodynamic equilibrium and their behavior is very much non-linear. This is a fundamental problem since adequate physical and mathematical bases for a sound analysis of these highly non-linear and non-equilibrium effects do not exist. Another (more practical) reason why a quantitative evaluation of the structure-property relationship of materials is hampered has to do with statistics. Metrological considerations of quantitative electron microscopy of crystalline materials pose some relevant questions to the statistical significance of the electron microscopy observations. In particular, in situations where there is only a small volume fraction of defects present or where there is a very inhomogeneous distribution, statistical sampling may be a problem.

Nevertheless, the situation is not hopeless because in situ rather than post mortem observations are now feasible. For a long time, a major drawback of experimental and theoretical research in the field of dislocations and grain boundaries has been that most of the work has been concentrated on static structures. Obviously, the dynamics of moving dislocations and grain boundaries are more relevant to the deformation of metals. Nuclear spin relaxation methods in the rotating frame have been developed as a complementary tool for studying dislocation dynamics in metals [2]. A strong advantage of this technique is that it detects dislocation motion in the bulk of the material, in contrast to in situ transmission electron microscopy, where the behavior of dislocations may be affected by image forces due to the proximity of free surfaces. However, information about the local response of dislocations to an applied stress cannot be obtained by nuclear spin relaxation and therefore in situ transmission electron microscopy remains a valuable tool in the study of dislocation dynamics. Direct observation of dislocation-grain boundary interactions during indentation has recently become possible through in situ nanoindentation in a transmission electron microscope. In this paper, results obtained with this technique are presented, the results pertaining to the study of deformation mechanisms in Al and Al–Mg alloys with grain sizes of the order of a few hundred nanometers.

The observation of the plastic deformation introduced by conventional nanoindentation has been restricted to post mortem studies of the deformed material, mostly by atomic force microscopy, indenter-based scanning probe microscopy, or scanning or transmission electron microscopy. This post mortem approach entails some significant limitations to the analysis of the deformation mechanisms. Most importantly, it does not allow for direct observation of the microstructure during indentation and thus lacks the possibility to monitor the precise nature of the deformation events and the evolution of dislocation structures as the indentation proceeds. Moreover, the deformed microstructure observed after indentation is generally different from that of the material under load, due to recovery during and after unloading. In the case of post mortem analysis by transmission electron microscopy, the preparation of the indented surface in the form of a thin foil often leads to mechanical damage to the specimen or relaxation of the stored deformation due to the proximity of free surfaces, thereby further obscuring the indentation-induced deformation.

The recently developed technique of in situ nanoindentation in a transmission electron microscope [3–8] does not suffer from these limitations and allows for direct observation of indentation phenomena. Furthermore, as the indenter can be positioned on the specimen accurately by guidance of the TEM, regions of interest such as particular crystal orientations or grain boundaries can be specifically selected for indentation. In situ nanoindentation measurements [8] on polycrystalline aluminum films have provided experimental evidence that grain boundary motion is an important deformation mechanism when indenting thin films with a grain size of several hundreds of nanometers. This is a remarkable observation, since stress-induced grain boundary motion is not commonly observed at room temperature in this range of grain sizes.

Grain boundary motion in metals typically occurs at elevated temperatures, driven by a free energy gradient across the boundary, which may be presented by the curvature of the boundary or stored deformation energy on either side of the boundary [9]. In the presence of an externally applied shear stress, it was found [10] that migration of both low-angle and high-angle grain boundaries in pure Al occurs at temperatures above 200 °C. This type of stress-induced grain boundary motion (known as dynamic grain growth) is considered by many researchers to be the mechanism responsible for the extended elongations obtained in

superplastic deformation of fine-grained materials. The occurrence of grain boundary motion in room temperature deformation of nanocrystalline fcc metals was anticipated recently by molecular dynamics simulations [11] and a simple bubble raft model [12]. Experimental observations of such grain boundary motion have subsequently been provided by in situ straining experiments of nanocrystalline Ni thin films [13] and in situ nanoindentation of nanocrystalline Al thin films [14]. In both the simulations and the experiments, grain boundary motion was observed for grain sizes below 20 nm. Dislocation mobility is greatly restricted at such grain sizes and other deformation mechanisms become more relevant. In contrast, the grain size for which grain boundary motion was found by in situ nanoindentation [8] was of the order of 200 nm. In simple deformation modes such as uniform tension or compression, dislocation-based plasticity is still predominant in this regime and grain boundary motion generally does not occur. In the case of nanoindentation however, the stress field is highly inhomogeneous and consequently involves large stress gradients [15]. These stress gradients are thought to be the primary factor responsible for the observed grain boundary motion at room temperature. Another aspect that may contribute to the occurrence of this phenomenon is the specific geometry of the in situ indentation specimens, which will be discussed in Section ''In situ nanoindentation in a TEM''.

We have focused on the indentation behavior of Al–Mg films and the effect of Mg on the deformation mechanisms described above. To this end, in situ nanoindentation experiments have been conducted on ultrafine-grained Al and Al–Mg films with varying Mg contents [16, 17]. The classification ''ultrafine-grained'' in this respect is used for materials having a grain size of the order of several hundreds of nanometers. In this paper, the TEM observations are interpreted and related to quantitative load-displacement data, both directly from the in situ indentation experiments and indirectly through conventional ex situ nanoindentation on the same specimens.

In situ nanoindentation in a TEM

In situ nanoindentation inside a TEM requires a special specimen stage designed to move an indenter towards an electron-transparent specimen on the optic axis of the microscope. The first indentation holder was developed in the late 1990s by Wall and Dahmen [3, 4] for a high-voltage microscope at the National Center for Electron Microscopy (NCEM) in Berkeley, California. In the following years, several other stages were constructed at NCEM with improvements made to the control of the indenter movement but without a transducer dedicated to measuring load and displacement. In the work described in this paper, two stages were used: a homemade qualitative holder constructed at NCEM for a JEOL 200CX microscope [5] and a prototype quantitative holder developed at Hysitron by Hysitron personnel (Hysitron, Inc., Minneapolis, MN) in collaboration with NCEM for a JEOL 3010 microscope. The latter holder is the first to accomplish in a TEM what is commonly referred to as depth-sensing indentation.

Certain design aspects of both holders are roughly the same. A piezoelectric tube allows high-precision movement of the tip in three dimensions, the indentation direction being perpendicular to the electron beam. Coarse positioning is provided by manual screw drives that move the indenter assembly against the vacuum bellows. The indenter itself is a Berkovich-type diamond tip, which is boron-doped in order to be electrically conductive in the TEM. The goniometer of the TEM provides a single tilt axis, so that suitable diffraction conditions can be set up prior to indentation.

In the case of the qualitative holder, the indenter tip is mounted directly to the piezo tube. The motion of the indenter into the specimen during indentation is accomplished by manual control of the voltage applied to the tube, which is recorded together with the TEM image. Since the compliance of the load frame is relatively high, the actual displacement of the indenter into the material depends not only on the applied voltage, but also to a certain extent on the response of the material. Consequently, this indentation mode is neither load- nor displacement-controlled. If the complex response of the piezo tube were fully known, the load could be calculated at any time during indentation from the motion provided by the piezo tube, the displacement of the indenter tip (which can be determined directly from the TEM image if in bright-field mode) and the compliance of the load frame [18]. Ideally, the correlation between the applied voltage and the displacement of the piezo element is linear. However, hysteresis, creep and saturation effects lead to significant nonlinearities. Moreover, as lateral motion is achieved by bending the tube, the state of deflection strongly affects the response in the indentation direction as well. Calibration measurements of the piezo response in vacuum at 12 points across the lateral range showed an average proportionality constant of 0.12 μm/V with a standard deviation as large as 0.04 μm/V. Although during indentation the

deflection of the tube is approximately constant and the response becomes more reproducible, the above-mentioned hysteresis, creep and saturation effects still complicate the measurement of the load. The implementation of a dedicated load-displacement transducer, as in the new prototype holder, is therefore essential for obtaining reliable quantitative indentation data (see for a comparison also [6]).

In the case of the quantitative holder, the indenter tip is mounted to a miniature transducer coupled to the piezo tube. Here, the piezo tube functions only as a fine positioner and is held static during indentation to avoid the previously described complications. By capitalizing upon its electrostatic actuation and capacitive displacement sensing capabilities, the transducer is able to deliver calibrated loads in excess of 1300 μN and measured displacements up to 5000 nm. Load and displacement noise floors are found to be ~0.1 μN and ~0.4 nm in the JEOL 3010 microscope. By adopting a parallel loading configuration and a very stiff load frame, the displacement signal generated by the transducer is a direct measure of the penetration depth. This displacement signal is inputted into a digital feedback system operating at a feedback loop rate of 22 kHz. The primary purpose of the feedback system is to control the electrostatic actuation voltage to the transducer with the aid of a proportional-integral-derivative (PID) algorithm [19] to meet the displacement demand, which also provides the benefit of damping the transducer in the high vacuum environment of the TEM, resulting in a settling time reduction by a factor of ~5000. The indentation is therefore displacement-controlled and can be programmed to follow a predefined displacement profile as a function of time. The in situ indentation load-displacement curves presented in this paper have all been produced with this displacement-controlled holder.

The geometry of the specimens used for in situ nanoindentation has to comply with two basic requirements: (i) an electron-transparent area of the specimen must be accessible to the indenter in a direction perpendicular to the electron beam, and (ii) this area of the specimen must be rigid enough to support indentation without bending or breaking. A geometry that fulfills both these requirements is a wedge that is truncated to a cap width large enough to provide the necessary rigidity while still allowing the electron beam to pass through. For the present investigation, we used wedge specimens prepared by bulk silicon micro-machining. Using this technique, wedge-shaped protrusions are routinely prepared on Si (001) substrates with a resolution of the order of 1 μm. The side planes of the ridge are aligned with {111} planes of the silicon crystal, so that repeated annealing and oxide removal subsequently leads to sharpening of the wedge driven by a reduction of the surface energy. In this way, a cap width of the order of 100 nm can be achieved. The ridge has a length of 1.5 mm and a height of 23 μm above the substrate. The included angle between the {111} side planes is 54.7°.

The silicon ridge specimen geometry provides a means to investigate any material that can be deposited as a thin film onto the silicon substrate. Metals with a low atomic number such as aluminum are particularly suitable for this purpose, since films of these metals can be made to several hundreds of nanometers thickness and still be transparent at the cap of the wedge to electrons with typical energies of 200–300 keV, as schematically depicted in Fig. 1a. An example of a resulting TEM image is shown in Fig. 1b.

Experimental procedure

The Al and Al–Mg films for the present investigation were deposited by thermal evaporation. The substrate was kept at 300 °C to establish a grain size of the order of the layer thickness, which was 200–300 nm for all specimens. After evaporation, the substrate heating was switched off, allowing the specimen to cool down to room temperature in approximately one hour. One pure Al film was prepared by evaporating a high purity (5 N) aluminum source. Deposition of the Al–Mg alloy films was achieved by evaporating alloys with varying Mg contents. Since Al and Mg have different melting temperatures and vapor pressures, the Mg content of the deposited film is not necessarily equal to that of the evaporated material. Moreover, the actual evaporation rates depend on the quality of the vacuum and the time profile of the crucible temperature. The composition of the deposited alloy films was therefore determined by energy dispersive spectrometry (EDS) in a scanning electron microscope at 5 kV. The measured Mg concentrations of the four Al–Mg films prepared were 1.1, 1.8, 2.6 and 5.0 wt%.

Since the solubility level of Mg in Al is 1.9 wt% at room temperature [20], β' and β precipitates were formed in the 2.6 and 5.0 wt% Mg specimens due to the relatively long cooling time. The attainable image resolution in the indentation setup was not high enough to resolve these precipitates, being compromised by the thickness of the specimen and possibly by the fact that the electron beam travels very closely to the substrate over a large distance. Nevertheless, the presence of precipitates both in the matrix and at the grain boundaries could be confirmed by strain contrast

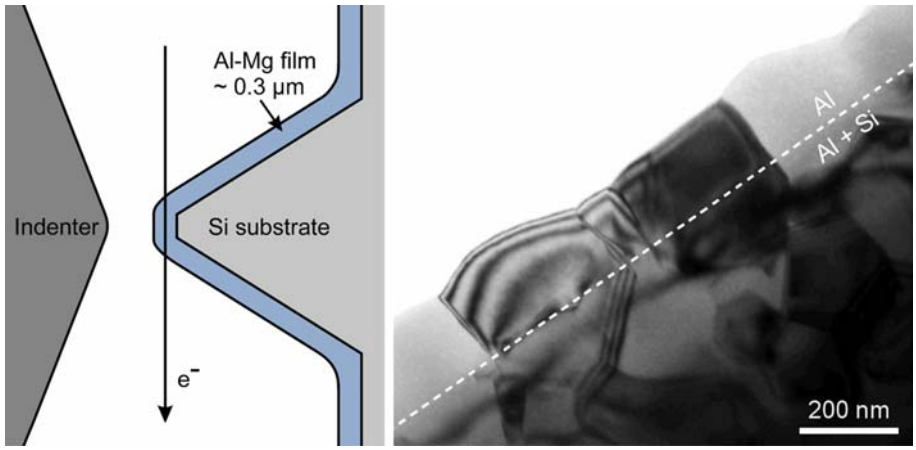

Fig. 1 (**a**) Schematic of in situ indentation setup. The deposited Al–Mg film is electron-transparent and accessible to the indenter at the tip of the Si wedge. (**b**) Typical bright-field image of a deposited film. The dashed line shows the top of the Si ridge

and distorted grain boundary fringes, respectively, which were not observed in the 1.1 and 1.8 wt% Mg specimens (Fig. 2). Furthermore, the presence of the brittle β phase on the grain boundaries leads to the appearance of intergranular cracks in the 2.6 and 5.0 wt% Mg specimens, as shown in the scanning electron micrographs in Fig. 3.

While Al deposited on a clean Si (001) surface may give rise to a characteristic mazed bicrystal structure due to two heteroepitaxial relationships [21], the Si substrates used in the present experiments were invariably covered with a native oxide film. Therefore, the orientations of the Al and Al–Mg grains of the film show no relation to that of the Si surface. An Electron Back Scatter Diffraction (EBSD) scan on the evaporated Al film showed a significant ⟨111⟩ texture (Fig. 4a), which can be explained by the fact that the surface energy of fcc materials has a minimum for this orientation. Furthermore, the EBSD measurements provided the distribution of the grain boundary misorientations (Fig. 4b), which shows that the grains are mostly separated by random high-angle grain boundaries with no significant preference for particular Coincidence Site Lattice (CSL) orientations.

On each of the evaporated films, three to four in situ experiments were carried out with maximum depths ranging from 50 to 150 nm, using the indentation stage for the JEOL 200CX. The indentation rate, being controlled manually through the piezo voltage, was of the order of 5 nm/s. In addition, several quantitative in situ indentation experiments were conducted with the prototype holder for the JEOL 3010 microscope on the Al and Al–2.6%Mg films. These displacement-controlled indentations were made to a depth of approximately 150 nm with a loading time of 20 s. In order to be able to resolve grain boundary phenomena during each in situ indentation, the specimen was tilted to such an orientation that two adjacent grains were both in (different) two-beam conditions.

Conventional nanoindentation measurements were carried out ex situ on the same films away from the wedge. As in the in situ experiments, a pyramidal Berkovich tip was used. Load-controlled indentations were executed to maximum depths of 50, 100 and 150 nm at a targeted strain rate of 0.05 s^{-1}, defined as loading rate divided by load. At this strain rate the indenter velocity during loading was of the order of 2 nm/s, which is comparable to the in situ measurements.

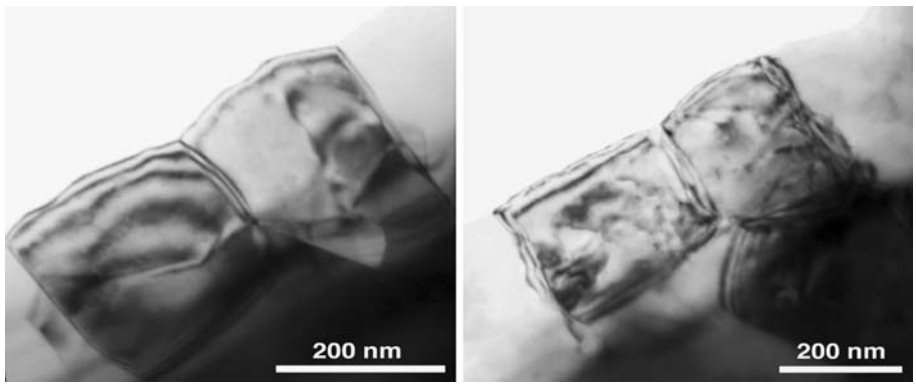

Fig. 2 Bright-field images of evaporated Al–Mg layers with (**a**) 1.1 and (**b**) 5.0 wt% Mg. The presence of Al–Mg precipitates in (**b**) is revealed by strain contrast

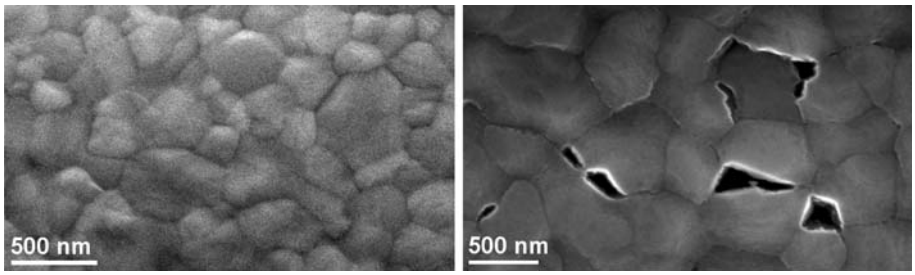

Fig. 3 Scanning electron micrographs of (**a**) pure Al film and (**b**) Al–5.0%Mg film away from the ridge. Cusped grain boundaries give rise to considerable surface roughness in both films. Grain boundary embrittlement by β precipitates leads to the appearance of intergranular cracks in the Al–5.0%Mg film

Dislocation dynamics in Al and Al–Mg thin films

The effect of Mg on the propagation of dislocations is particularly visible during the early stages of loading. While, in the case of pure Al, the dislocations instantly spread across the entire grain (i.e. faster than the 30 frames per second video sampling rate), they advance more slowly and in a jerky type fashion in all observed Al–Mg alloys. Figure 5 shows a sequence of images from an indentation in Al–2.6%Mg. The arrows mark the consecutive positions where the leading dislocation line is pinned by solutes. From these images, the mean jump distance between obstacles is estimated to be of the order of 50 nm. Due to the single-tilt axis limitation of the indentation stage, the orientation of the slip plane relative to the electron beam is unknown; therefore, the measured jump distance is a projection and a lower bound of the actual jump distance.

At the low strains for which jerky-type dislocation motion is observed, solute atoms are the predominant barriers to mobile dislocations, as has been shown in earlier in situ pulsed nuclear magnetic resonance (NMR) experiments [2, 22, 23]. Consequently, the mean jump distance can be predicted by Mott-Nabarro's model of weakly interacting diffuse forces between Mg solutes and dislocations in Al [24]. A calculation of the effective obstacle spacing, assuming that the maximum internal stress around a solute atom has a logarithmic concentration dependence, yields a value of 30 nm in Al–2.6%Mg. This is in fair agreement with our experimental observation of a mean jump distance of the order of 50 nm.

Besides solute atoms, (semi-)coherent β'/β precipitates in Al–Mg alloys can also provide significant barriers to dislocation motion. As aforementioned, the mean spacing of these precipitates could not be measured very accurately due to the limited resolution of the microscope combined with the specific indentation stage. However, we can make an estimate based on the solid solubility of magnesium in Al at room temperature of 1.9 wt%. The calculated volume fraction f_V is 2.4 % for the β phase at 300 K. The mean planar separation, which is a relevant measure for the interaction of a gliding dislocation with a random array of obstacles in its slip plane, is given by [25]

$$\lambda \cong \frac{2\sqrt{2}\pi r}{3f_V} \tag{1}$$

provided that the size of the particles r is negligible in comparison with their center-to-center separation, i.e. if $\lambda >> r$. It is reasonable to assume that the minimum

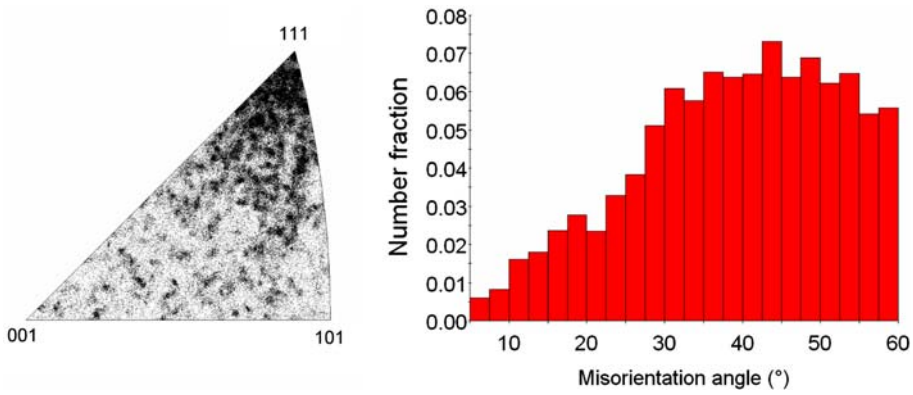

Fig. 4 Results obtained from an EBSD scan on the pure Al film: (**a**) discrete pole figure showing the ⟨111⟩ texture of the evaporated film; (**b**) distribution of the grain boundary misorientation angle

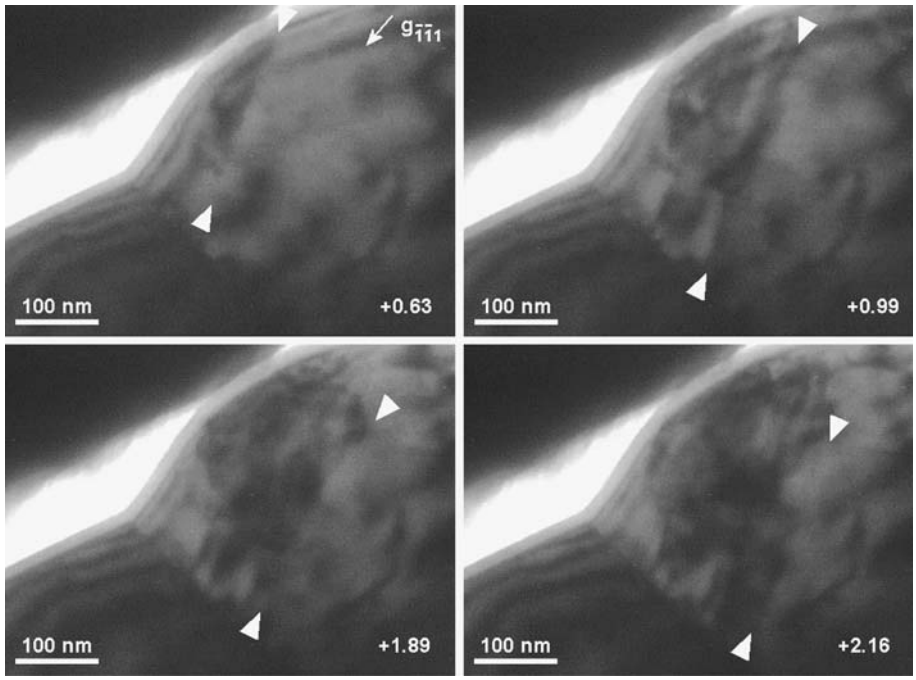

Fig. 5 Series of bright-field images showing jerky motion of dislocations during indentation of Al–2.6wt%Mg. The time from the start of the indentation is given in seconds. Note the presence of a native oxide layer on the surface [17]

size of the semicoherent precipitates is at least 10 nm to produce sufficient strain contrast in Fig. 2b. As a result, the mean planar separation of the precipitates is calculated to be at least 92 nm, i.e. larger than the mean separation between the solutes. In this approach, the obstacles are assumed to be spherical and consequently we ignore the effect that the precipitation in Al may become discontinuous or continuous depending on the temperature. However, even in the case of a Widmanstätten structure, the effective separation between the needle-shaped precipitates is larger than the effective solute obstacle spacing [26]. Therefore, based on the experimental observations in the alloys below and above the solid solubility of magnesium, the strain contrast depicted in Fig. 2b and the abovementioned theoretical considerations, solute atoms are assigned as the main obstacles to dislocation motion.

A considerable part of the research effort on Al–Mg alloys has been devoted to understanding the pronounced, repeated yielding that occurs during plastic deformation of these alloys. The physical basis for this phenomenon, known as the Portevin–Le Châtelier (PL) effect or serrated yielding [27], is a negative strain rate sensitivity of the flow stress, caused by interaction between dislocations and mobile solute atoms [28]. This self-repeating process consists of pinning of the dislocations by the solutes, the breakaway of the dislocations from the solutes, and diffusion of the solute atoms to the dislocations, which are consequently pinned again. In uniaxial deformation, the most characteristic features of the PL effect are serrations, i.e. stress drops or steps, in the stress-strain curve. The PL effect in Al–Mg has been investigated in several deformation modes, including depth-sensing indentation [29, 30]. The associated dislocation dynamics have been characterized by in situ straining in a high-voltage electron microscope [31, 32] and pulsed NMR experiments [2, 22, 23].

The repeated yielding due to the PL effect occurs within specific limits of temperature, strain, strain rate and impurity concentration. Based on the theoretical model by Kubin and Estrin [33], Chinh et al. [30] calculated a minimum concentration of 0.62 wt% Mg for instabilities to occur in binary Al–Mg at room temperature. The strain required for serrated yielding to start during indentation depends on the Mg concentration; an estimate for the equivalent indentation depth can be obtained from the following empirical relation for Vickers indentation of bulk Al–Mg [30]:

$$h_c = A(C - C_0)^n \tag{2}$$

where A = 2.91 μm, C_0 = 0.86 wt% and n = –0.23 are the fitting parameters experimentally determined at a loading rate of 14 mN/s. Given that the critical load P_c at which the instabilities start is proportional to the loading rate ζ [29], we have

$$h_c \propto \sqrt{P_c} \propto \sqrt{\zeta} \tag{3}$$

Assuming an average loading rate in the present experiments of 0.03 mN/s, we find a critical depth

ranging from 0.10 μm for Al–5.0%Mg to 0.19 μm for Al–1.1%Mg. This is consistent with the results from the ex situ quantitative indentations, as will be shown in the next section.

In situ straining studies in a TEM have related the PL effect to sudden activation, multiplication and coordinated motion of dislocations [31, 32]. Such behavior was not observed in our in situ experiments. Moreover, the indentation depths at which dislocation motion was studied were considerably lower than the estimated critical depths as obtained above. Therefore, it is concluded that the jerky motion observed in situ is due to solute drag without appreciable diffusion of solute Mg.

The extraction of mechanical properties from the quantitative indentation measurements on the evaporated thin films was compromised by the surface roughness and the grain size at shallow depths and by the film thickness at deeper depths. Recent numerical studies [34, 35] suggest that for a soft film on a hard substrate, the influence of the substrate may not be appreciable until the depth exceeds one half of the film thickness. Still at these relatively high indentation depths, the probed volume was not sufficiently large to give reliable hardness and modulus data. As illustrated in Fig. 3, most of the films show considerable surface roughness due to cusps at the grain boundaries. This leads to an ill-defined contact area during initial loading. Furthermore, the size of the indents was of the order of the grain size, causing scatter in the indentation results due to microstructural variations. For these reasons, our analysis of the quantitative data focuses on characteristic features of the load–displacement curves and their relation to the in situ observations, rather than on the calculation of hardness and elastic modulus.

The ex situ load-controlled indentation measurements on the pure Al film showed abrupt displacement bursts during loading up to a depth of around 70 nm, as illustrated in Fig. 6a. Between the bursts, the slope of the loading curve increases continuously. No such discontinuities were observed in indentations of any of the Al–Mg films, as illustrated in Fig. 6b showing loading curves of the Al–2.6%Mg film. As would be expected from the critical indentation depths for the PL effect obtained in the previous section, no pronounced serrated yielding was observed in the Al–Mg films during indentation to 150 nm depth, except for the Al–5.0%Mg film (Fig. 6c). Indeed in this case, the serrations start between 80 and 100 nm depth as predicted by the calculations. The initially ''soft'' response of the Al–Mg films during the first tens of nanometers can be attributed to their surface roughness.

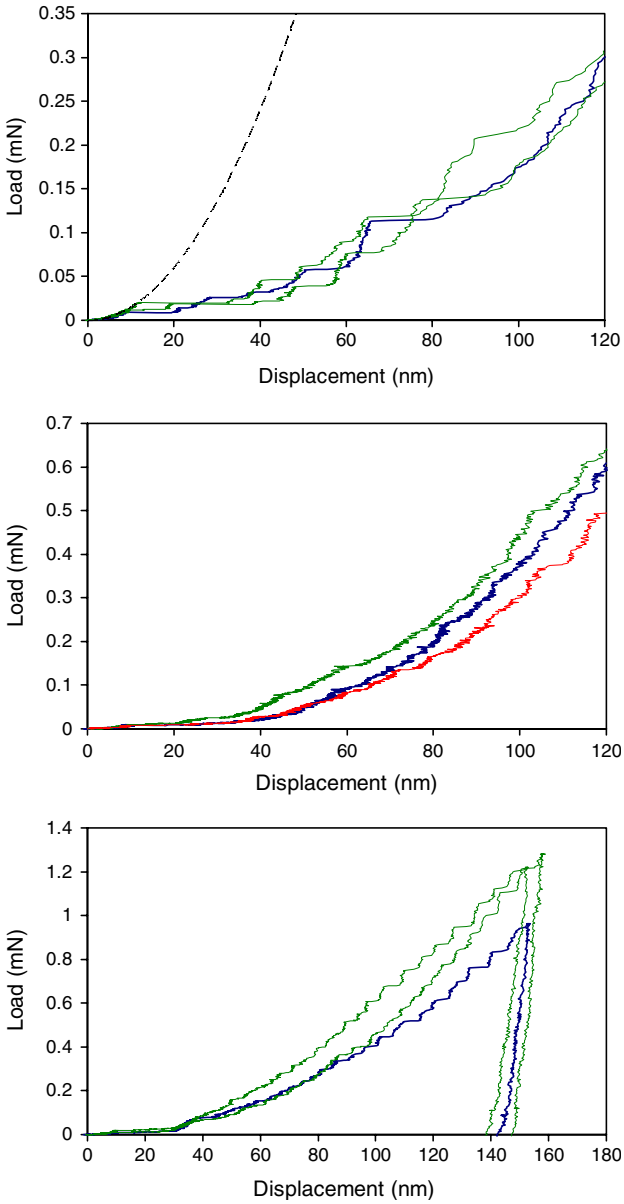

Fig. 6 (**a**) Loading curves for ex situ load-controlled indentations on pure Al film, showing discrete displacement jumps. The dashed line represents Berkovich indentation of an elastic material with $E_r = 74$ GPa. (**b**) Loading curves without pronounced yield excursions for indentations in Al–2.6%Mg film. (**c**) Serrated yielding during indentation of Al–5.0%Mg film

Analysis of the curvature of the loading portions prior to the first excursion and between subsequent excursions in the pure Al film shows that these are well described by elastic loading by a sharp Berkovich indenter although a perfectly sharp Berkovich indenter is not expected to yield purely elastic loading. The yield behavior is classified as staircase yielding due to sudden dislocation nucleation and propagation. Staircase yielding has been reported for indentation of both single crystal and polycrystalline Al thin films [36]. The

absence of these yield events during indentation of Al–Mg films, both below and above the solubility limit, shows that initial plasticity is significantly affected by solute Mg. Presumably, solute drag prevents dislocation bursts from propagating through the crystal, i.e. the stored elastic energy is insufficient to push a series of dislocations through the solute atmosphere at constant indentation load. As the load increases further, some of the available dislocations are able to overcome the force associated with solute pinning, thereby allowing plastic relaxation to proceed smoothly. Since there is no collective motion of dislocations as in pure Al, the measured loading response is essentially continuous. This perception is supported by the extensive solute drag observed in situ.

Interestingly, the difference in initial yield behavior between the pure Al and Al–Mg films was not observed in the quantitative displacement-controlled indentations performed in situ. Figure 7a shows the data recorded during an indentation on pure Al. The loading curve shows pronounced load drops, which have the same physical origin as the displacement excursions in load-controlled indentation, i.e. stress relaxation by bursts of dislocation activity. Also in this case, the loading behavior up to the first load drop appears to follow closely the elastic Berkovich response although this comparison may not be entirely valid because of irregularities on the tip surface as observed in TEM. In contrast with the ex situ load-controlled indentations, the measured response of Al–Mg follows roughly the same behavior (Fig. 7b): load drops occur with approximately the same size and frequency as in pure Al. These observations illustrate that while the physical mechanism underlying the instabilities in load-controlled and displacement-controlled indentation are the same, the criteria for them to occur may depend on the indentation mode used. One rationale for this difference may be as follows. When the critical shear stress for a dislocation source under the indenter is reached under load control, a significant strain burst results only if the source is able to generate many dislocations at constant load. This again is possible only if the newly nucleated dislocations can freely propagate through the lattice, as in pure Al. Under displacement control however, the feedback system reduces the load during a yield event so as to keep the error in the constant displacement rate minimal. The observed instabilities in particular lead to large and rapid changes in contact stiffness, which are very challenging from the perspective of feedback control. If the feedback bandwidth is sufficiently high, the system may respond to the decrease in contact stiffness when only a few

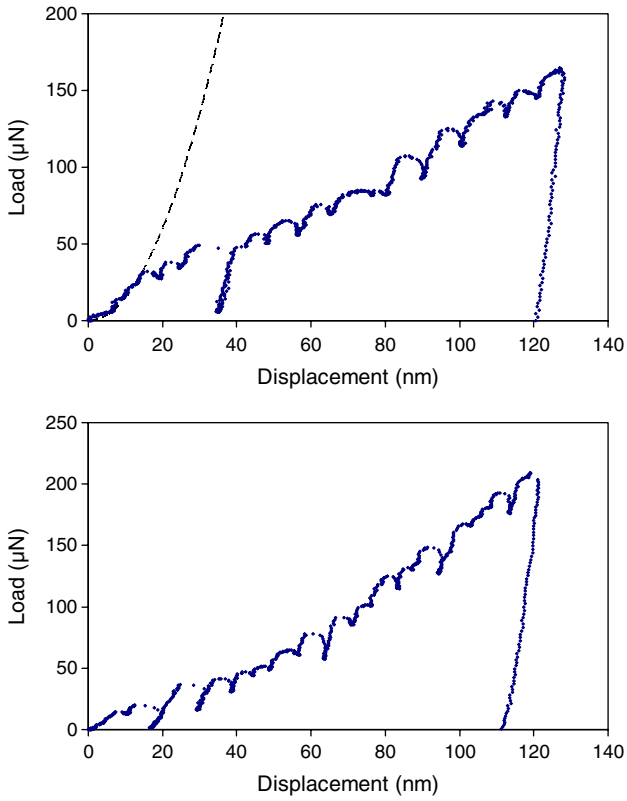

Fig. 7 Displacement-controlled indentation behavior measured in situ on (**a**) pure Al and (**b**) Al–2.6%Mg. The load drops in both materials are similar

dislocations are nucleated; in this case, the occurrence of a detectable load drop does not require collective propagation of many dislocations and as such may be observed under solute drag conditions as well. Warren et al. [19] reported that the density of load drops in displacement-controlled indentation of an Al (100) surface is significantly higher than that of displacement bursts in load-controlled indentation of the same surface, demonstrating that the former is indeed a more sensitive technique to detect discontinuous yielding than the latter. Moreover, displacement control allows for the natural process of load relaxation whereas load control involves an additional input of energy to compensate for the load relaxation. Consequently, a single pronounced displacement burst in load control might be the equivalent of a series of load drops in displacement control, which means the frequency of discrete events can be significantly higher in displacement control than in load control. Besides the indentation control mode, also the loading rate may affect the initial yield phenomena to some extent, especially in the case of Al–Mg alloys where strain-induced diffusion of Mg is appreciable.

The quantitative in situ indentations show a considerable amount of dislocation activity prior to the first macroscopic yield point. These observations provide strong evidence in support of the claim that dislocations are nucleated prior to the first detectable yield point in the load–displacement curve [37–39]. The loading behavior may consequently be classified as quasi-plastic, since only limited plasticity occurs at this stage. In the present in situ experiments, the geometry of the indenter tip is not so accurately defined as to conclusively validate the correspondence of the loading curve to purely elastic loading. Furthermore, the geometry and the microstructure of the specimens may affect the nucleation behavior through the presence of nearby grain boundaries and free surfaces. To further clarify the dislocation dynamics at this initial stage of nanoindentation, in situ experiments on more carefully defined systems have recently been conducted (Minor et al., submitted).

Grain boundary dynamics in Al and Al–Mg thin films

To confirm the occurrence of grain boundary movement in aluminum as had been reported earlier [8], several in situ indentations were performed near grain boundaries in the pure Al film. Indeed, significant grain boundary movement was observed for both low and high-angle boundaries. This is illustrated in Fig. 8 by image frames of subsequent stages of the loading part of an indentation near a high-angle boundary. After initial contact (Fig. 8a) and plastic deformation of grain B (Fig. 8b), both grain boundaries outlining grain B move substantially (Figs. 8c,d). By comparing dark-field images taken before and after the indentation, as shown in Fig. 9, the grain boundary shifts are measured to be 0.04 μm for the left boundary and 0.22 μm for the right boundary. Of course it should be realized that the present results show the two dimensional projection of 3D deformation processes.

It should be emphasized that the observed grain boundary motion is not simply a displacement of the boundary together with the indented material as a whole; the boundary actually moves through the crystal lattice and the volume of the indented grain changes accordingly at the expense of the volume of neighboring grains. The trends observed throughout the indentations suggest that grain boundary motion becomes more pronounced with decreasing grain size and decreasing distance from the indenter to the boundary. Moreover, grain boundary motion occurs less frequently as the end radius of the indenter increases due to tip blunting or contamination. Both these observations are consistent with the view that the motion of grain boundaries is promoted by high local stress gradients as put forward in the introduction of this paper. The direction of grain boundary movement can be both away from and towards the indenter, and small grains may even completely disappear under indentation [14]. Presumably, the grain boundary parameters play an important role in the mobility of an individual boundary, since the coupling of the indenter-induced stress with the grain boundary strain field depends strongly on the particular structure of the boundary.

The quantitative in situ indentation technique offers the possibility to directly relate the observed grain boundary motion to features in the load-displacement curve. While this relationship has not been thoroughly studied in the present investigation, preliminary results suggest that the grain boundary motion is associated with softening in the loading response. Softening can physically be accounted for by the stress relaxation that occurs upon grain boundary motion. However, the quantification of overall mechanical behavior is complicated by the frequent load drops at this stage of indentation, and further in situ indentation experiments are needed to investigate this phenomenon more systematically and quantitatively.

The movement of grain boundaries as observed in Al was never found for high-angle boundaries in any of the Al–Mg specimens, even when indented to a depth greater than half of the film thickness. Figure 10 shows a sequence of images from an indentation on an Al–1.8%Mg layer. At an indentation depth of approx. 85 nm into grain B (Fig. 10c), plastic deformation is initiated in grain A by transmission across the grain boundary. However, no substantial grain boundary movement occurs; small grain boundary shifts (~10 nm) that were measured occasionally can be attributed to displacement of the material under the indenter as a whole, with conservation of grain volume, rather than to actual grain boundary motion (Fig. 11). Our observations as such indicate a significant pinning effect of Mg on high-angle grain boundaries in these alloys.

In contrast to high-angle grain boundaries, the mobility of low-angle boundaries in Al–Mg was found to be less affected by the presence of Mg. This is illustrated by the rapid disintegration of a low-angle tilt boundary in Al–5.0%Mg as shown in Fig. 12. At a relatively low indentation depth of about 20 nm, the dislocations that were initially confined to the indented grain spread across both grains without being visibly obstructed by the tilt boundary. The boundary effectively disappears at this point with the end result of the two grains becoming

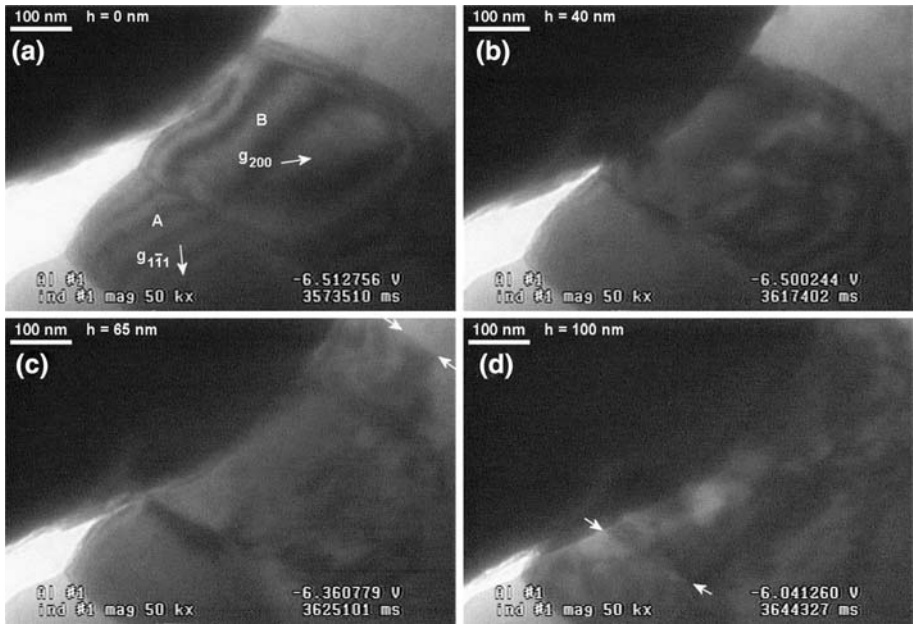

Fig. 8 Series of bright-field images from an indentation on Al, which is accommodated by movement of the grain boundaries (marked with arrows). The approximate indentation depth h is given in each image [17]

one. Figures 13a–c show the orientation of the two grains before indentation. The grains share the same ⟨112⟩ zone axis, but are in different two-beam conditions due to their slight misorientation (~0.7°). Figure 13d shows the grains after the indentation to be both in the same diffracting condition as the grain in Fig. 13a.

Ideally, in order to compare the observed grain boundary behavior between different measurements, the indenter-induced stress at the boundary should be known. However, due to surface roughness, tip imperfections and the complicated specimen geometry, it is difficult to accurately measure or calculate the local stress fields. Comparisons between different measurements are

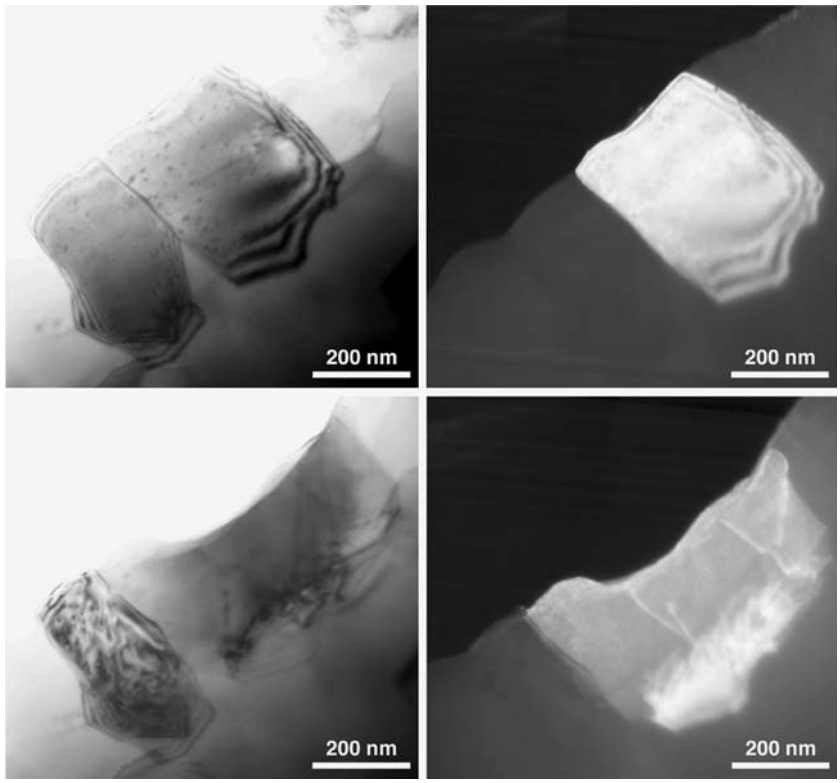

Fig. 9 Bright- and dark-field images of the indented grain (**a**, **b**) before and (**c**, **d**) after the indentation depicted in Fig. 8. Grain boundary motion leads to a significant volume increase of the indented grain

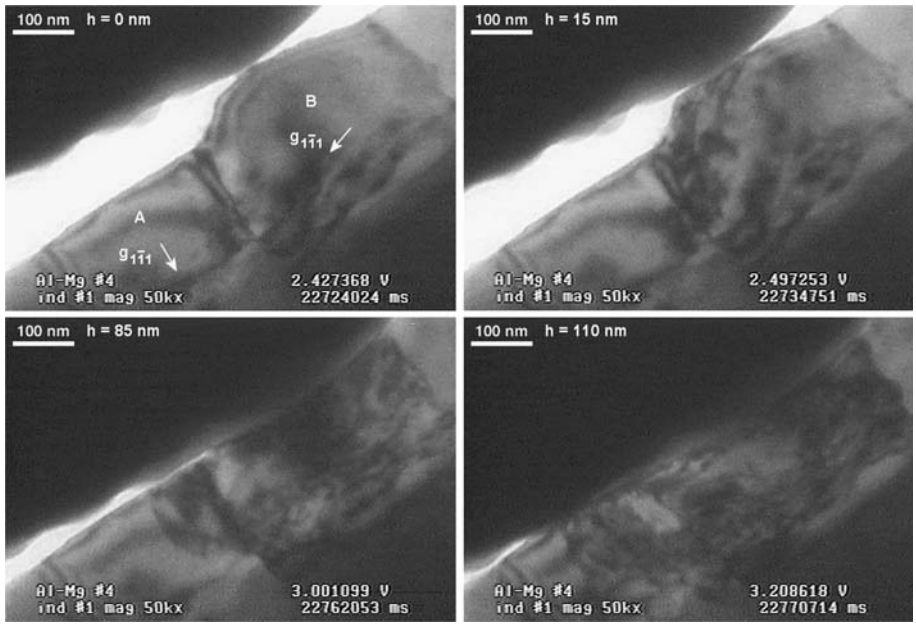

Fig. 10 Series of bright-field images from an indentation on Al–1.8%Mg. No movement of the high-angle grain boundaries is observed [17]

therefore mainly based on indentation depth. Our observation of grain boundary pinning in Al–Mg in this context means that no motion of high-angle boundaries was observed in Al–Mg in more than fifteen indentations to a depth of the order of 100 nm, while in pure Al, grain boundary motion was frequently observed at indentation depths of 50 nm or less.

The Al–Mg films used in this study include compositions both below and above the solubility limit of Mg in Al. However, no differences in indentation behavior between the solid solution and the precipitated microstructures were observed. Consequently, the observed pinning of high-angle boundaries in Al–Mg is attributed to solute Mg. The pinning is presumably due to a change in grain boundary structure or strain fields caused by solute Mg atoms on the grain boundaries. Relatively few direct experimental observations have been reported on this type of interaction. Sass and co-workers observed that the addition of Au and Sb impurities to bcc Fe changes the dislocation structure

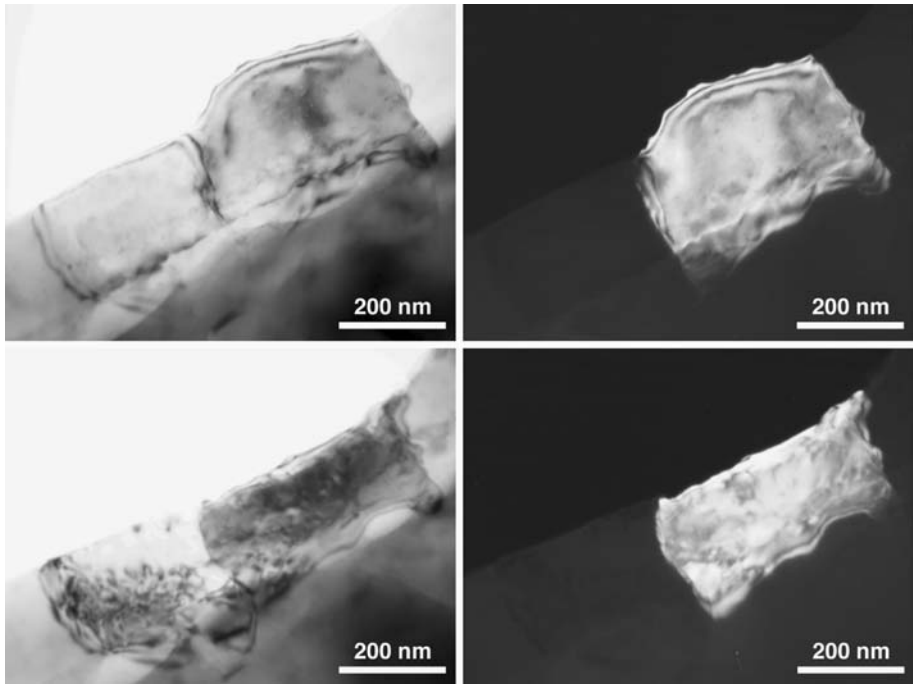

Fig. 11 Bright- and dark-field images of the indented grain (**a**, **b**) before and (**c**, **d**) after the indentation shown in Fig 10. Apart from a slight displacement of the boundaries due to the shape change of the indented grain, no significant grain boundary motion is detected

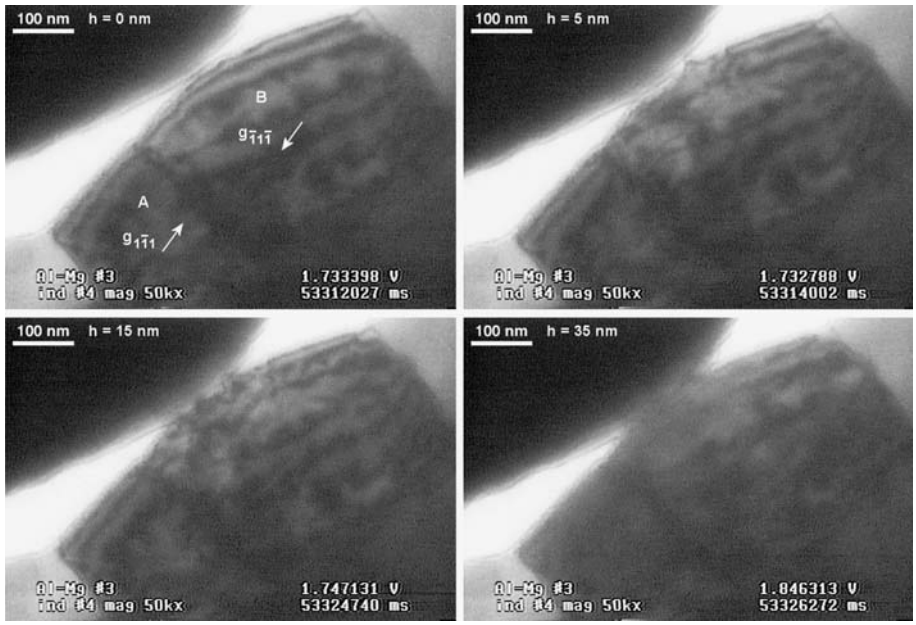

Fig. 12 Series of bright-field images from an indentation on Al–5.0%Mg, showing the disintegration of a low-angle ⟨110⟩ tilt boundary between (**c**) and (**d**)

of ⟨100⟩ twist boundaries of both low-angle [40] and high-angle [41] misorientation. Rittner and Seidman [42] calculated solute distributions at ⟨110⟩ symmetric tilt boundaries with different boundary structures in an fcc binary alloy using atomistic simulations. However, the influence of solutes on the structure of such boundaries has not been experimentally identified.

Possible changes in atomic boundary structure due to solute atoms may be observed by high-resolution TEM (HRTEM). Atomic-scale observation of grain boundaries using this technique requires that the crystals on both sides share a close-packed direction so that both lattices can be atomically resolved at the same time. The mazed bicrystal structure that forms

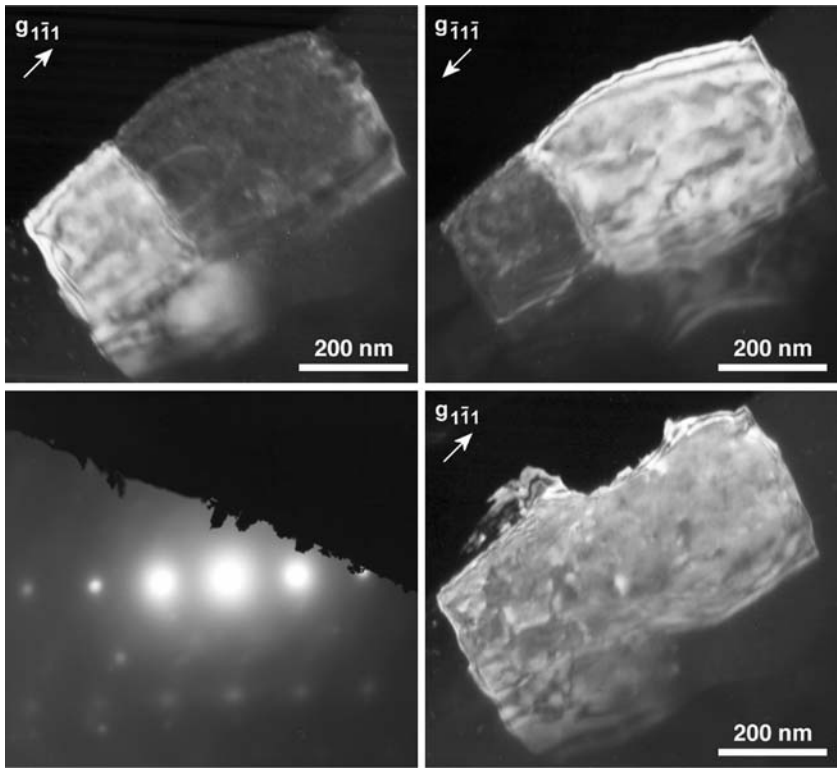

Fig. 13 (**a**, **b**) Dark-field images of the two Al–5.0%Mg grains shown in Fig. 12 before indentation. (**c**) Diffraction pattern showing the ⟨112⟩ orientation of both grains; the cut-off is due to the in situ specimen geometry. (**d**) Dark-field image after indentation [13]

when an Al film is deposited epitaxially onto a Si (001) surface meets this condition. The epitaxial relationships Al (110) // Si (001), Al [001] // Si [110] and Al (110) // Si (001), Al [001] // Si $[1\bar{1}0]$ lead to two possible orientations that are separated exclusively by 90° ⟨110⟩ tilt boundaries [21, 43]. The structure of such boundaries has been successfully studied in HRTEM studies of Al films on Si substrates [21, 44, 45] and Au films on Ge substrates [46–49], which exhibit the same epitaxial relationships. Moreover, the effect of alloying elements in Al has been explored by evaporating alloys such as Al–Cu and Al–Ag [50].

In order to study the effect of Mg on these tilt boundaries, we deposited Al and Al–Mg films onto Si (001) substrates that had been stripped of their native oxide film. Indeed, we found that in epitaxial films evaporated from pure Al, the 90° ⟨110⟩ tilt grain boundaries are facetted on $\{100\}_A//\{110\}_B$ and $\{557\}_A//\{557\}_B$ planes, which can be atomically resolved (Fig. 14a). The addition of Mg however drastically changes the microstructure of the deposited film: evaporation of Al–Mg on a Si substrate heated to 300 °C (which is necessary to reduce the lattice mismatch between Al and Si) leads to the formation of the intermetallic compound Mg_2Si, which prohibits any further epitaxial growth (Fig. 14b). Even in a two-step evaporation consisting of a pure Al deposition to provide a basis for the bicrystal structure and a subsequent Al–Mg deposition to introduce the Mg, the Mg diffuses to the substrate, driven by the reaction with the Si substrate. This method therefore could not be used to study the effect of Mg on the atomic structure of the grain boundaries.

Another effect that may contribute to the pinning of special boundaries is solute drag on extrinsic grain boundary dislocations (EGBDs) as reported by Song et al. [51], who showed that the dissociation rate of EGBDs in Al alloys is reduced by the addition of Mg. This implies that the indenter-induced deformation is accommodated more easily by these boundaries in pure Al than by those in Al–Mg.

The fact that low-angle grain boundaries were found to be mobile regardless of the Mg content can be explained by their different boundary structure. Up to a misorientation of 10–15°, low-angle boundaries can be described as a periodic array of edge and screw dislocations by Frank's rule [52]. In such an arrangement, the strain fields of the dislocations are approximated well by individual isolated dislocations and their interaction with an external stress field can be calculated accordingly. Since there is no significant interaction between the individual grain boundary dislocations, the stress required to move a low-angle boundary is much lower than for a high-angle boundary. Low-angle pure tilt boundaries consisting entirely of parallel edge dislocations are fully glissile and therefore particularly mobile. In general, a combination of glide and climb is required to move a low-angle boundary [53].

As a corollary, the structural difference between low and high-angle boundaries also affects the extent of solute segregation. Because solutes generally segregate more strongly to high-angle boundaries [54], the observed difference in mobility may partly be a compositional effect. EDS measurements were carried out and indeed showed an enhanced Mg concentration profile but because of the probe size and broadening of the beam inside the sample it is difficult to exclude the contributions from the grain interior. Therefore we cannot present yet hard evidence on this point.

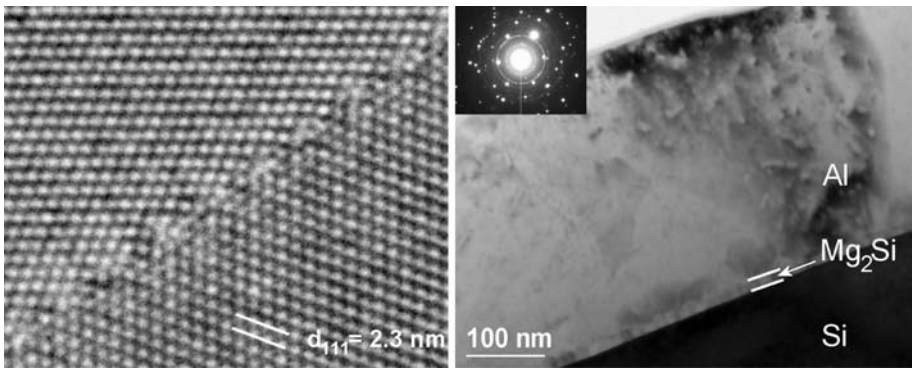

Fig. 14 (**a**) High-resolution micrograph of a 90° ⟨110⟩ asymmetrical tilt boundary in an epitaxial Al thin film, showing a periodic structure along the boundary plane. The orientation of the boundary plane is $\{100\}_A//\{110\}_B$. (**b**) Cross section of a film deposited from an Al–2.2 wt%Mg source onto a Si (001) substrate; the intermetallic compound Mg_2Si, identified by its diffraction ring pattern (inset), forms a 15 nm thick layer at the interface

Conclusions

The experiments presented provide insights into the nanomechanical behavior of Al and Al–Mg alloys at room temperature by making use of the novel technique of in situ nanoindentation in a TEM. The observed propagation of dislocations is markedly different between Al and Al–Mg films: the presence of solute Mg results in solute drag, evidenced by jerky dislocation motion with a mean jump distance that compares well to earlier theoretical and experimental results. It is proposed that this solute drag accounts for the difference in load-controlled indentation response between Al and Al–Mg alloys. Several yield excursions are observed during initial indentation of pure Al, which are commonly attributed to collective motion of dislocations nucleated under the indenter. These yield excursions are attenuated during indentation of the Al–Mg alloys; presumably, the solute drag prevents the elastic energy from being released in a sudden dislocation burst and thus smoothes out the initial indentation response. Displacement-controlled indentation does not result in a qualitative difference between Al and Al–Mg, which can be explained by the specific feedback characteristics providing a more sensitive detection of plastic instabilities and allowing the natural process of load relaxation to occur.

The in situ indentation measurements confirm grain boundary motion as an important deformation mechanism in ultrafine-grained Al when it is subjected to a highly inhomogeneous stress field as produced by a Berkovich indenter. It is found that solute Mg effectively pins high-angle grain boundaries during such deformation. The proposed mechanism for this pinning is a change in the atomic structure of the boundaries, possibly aided by solute drag on extrinsic grain boundary dislocations. The mobility of low-angle boundaries is not affected by the presence of Mg, which is attributed to their different boundary structure consisting of periodic dislocation arrangements.

Acknowledgements Indisputably Professor David Brandon became an inspiring and enthusiastic leader in the field of materials science. We are eager to seize this opportunity to thank him for his stimulus provided over the years and for his international leadership. The contributions of Daan Hein Alsem (LBNL–Berkeley) to the preparation of the Al–Mg thin films are gratefully acknowledged. The work is part of the research program of the Netherlands Institute for Metals Research, project nr MC4.01104. The quantitative in-situ nanoindentation holder was developed under a U.S. Department of Energy SBIR grant (DE-FG02–04ER83979) awarded to Hysitron, Inc., which does not constitute an endorsement by DOE of the views expressed in this article. This work also was supported by the Director, Office of Science, Office of Basic Energy Sciences, of the U.S. Department of Energy under Contract No. DE-AC02-05CH11231.

References

1. Brandon D, Wayne DK (1999) Microstructural characterization of materials. John Wiley, New York
2. De Hosson JThM, Kanert O, Sleeswyk AW (1983) In: Nabarro FRN (ed) Dislocations in solids, vol 6. North-Holland, Amsterdam, p 441
3. Wall MA, Dahmen U (1997) Microsc Microanal 3:593
4. Wall MA, Dahmen U (1998) Microsc Res Tech 42:248
5. Stach EA, Freeman T, Minor AM, Owen DK, Cumings J, Wall MA, Chraska T, Hull R, Morris JW Jr, Zettl A, Dahmen U (2001) Microsc Microanal 7:507
6. Minor AM, Morris JW Jr, Stach EA (2001) Appl Phys Lett 79:1625
7. Minor AM, Lilleodden ET, Stach EA, Morris JW Jr (2002) J Electron Mater 31:958
8. Minor AM, Lilleodden ET, Stach EA, Morris JW Jr (2004) J Mater Res 19:176
9. Doherty RD, Hughes DA, Humphreys FJ, Jonas JJ, Juul Jensen D, Kassner ME, King WE, McNelley TR, McQueen HJ, Rollett AD (1997) Mater Sci Eng A 238:219
10. Winning M, Gottstein G, Shvindlerman LS (2001) Mater Sci Eng A 317:17
11. Van Swygenhoven H, Caro A, Farkas D (2001) Mater Sci Eng A 309–310:440
12. Van Vliet KJ, Tsikata S, Suresh S (2003) Appl Phys Lett 83:1441
13. Shan Z, Stach EA, Wiezorek JMK, Knapp JA, Follstaedt DM, Mao SX (2004) Science 305:654
14. Jin M, Minor AM, Stach EA, Morris JW Jr (2004) Acta Mater 52:5381
15. Larsson P-L, Giannakopoulos AE, Söderlund E, Rowcliffe DJ, Vestergaard R (1996) Int J Solids Structures 33:221
16. Soer WA, De Hosson JThM, Minor AM, Stach EA, Morris JW Jr (2004) Mater Res Soc Symp Proc 795:U9.3.1
17. Soer WA, De Hosson JThM, Minor AM, Morris JW Jr, Stach EA (2004) Acta Mater 52:5783
18. Minor AM, Ph.D. thesis (University of California, Berkeley, 2002)
19. Warren OL, Downs SA, Wyrobek TJ (2004) Z Metallkd 95:287
20. Mondolfo LF (1979) Aluminum alloys: structure and properties. Butterworth, London 313
21. Dahmen U, Westmacott KH (1988) Scripta Metall 22:1673
22. Schlagowski U, Kanert O, De Hosson JThM, Boom G (1988) Acta Metall 36:865
23. De Hosson JThM, Kanert O, Schlagowski U, Boom G (1988) J Mater Res 3:645
24. Nabarro FRN (1975) In: Hirsch PB (ed) The physics of metals, vol 2. Cambridge University Press, p 152
25. Foreman AJE, Makin MJ (1966) Philos Mag 14:911
26. De Hosson, JThM, Alsem WHM, Tamler H, Kanert O (1983) In: Sih GC, Provan JW (eds) Defects, Fracture and Fatigue. Martinus Nijhoff, The Hague, p 23
27. McCormick PG (1972) Acta Metall 20:351
28. van den Beukel A (1980) Acta Metall 28:965
29. Bérces G, Chinh NQ, Juhász A, Lendvai J (1998) J Mater Res 13:1411
30. Chinh NQ, Csikor F, Kovács Zs, Lendvai J (2000) J Mater Res 15:1037
31. Tabata T, Fujita H, Nakajima Y (1980) Acta Metall 28:795
32. Robinson JM (1995) Mater Sci Eng A 203:238
33. Kubin LP, Estrin Y (1990) Acta Metall Mater 38:697
34. Chen X, Vlassak JJ (2001) Mater J Res 16:2974
35. Xu Z-H, Rowcliffe D (2004) Thin Solid Films 447–448:399

36. Gouldstone A, Koh H-J, Zeng K-Y, Giannakopoulos AE, Suresh S (2000) Acta Mater 48:2277
37. Gerberich WW, Venkataraman SK, Huang H, Harvey SE, Kohlstedt DL (1995) Acta Metall Mater 43:1569
38. Gerberich WW, Nelson JC, Lilleodden ET, Anderson P, Wyrobek JT (1996) Acta Mater 44:3585
39. Bahr DF, Kramer DE, Gerberich WW (1998) Acta Mater 46:3605
40. Sickafus K, Sass SL (1984) Scripta Metall 18:165
41. Lin CH, Sass SL (1988) Scripta Metall 22:735
42. Rittner JD, Seidman DN (1997) Acta Mater 45:3191
43. Lamelas FJ, Tang M-T, Evans-Lutterodt K, Fuoss PH, Brown WL (1992) Phys Rev B 46:15570
44. Dahmen U, Hetherington CJD, O'Keefe MA, Westmacott KH, Mills MJ, Daw MS, Vitek V (1990) Philos Mag Lett 62:327
45. Paciornik S, Kilaas R, Turner J, Dahmen U (1996) Ultramicroscopy 62:15
46. Pénisson JM, Lançon F, Dahmen U (1999) Mater Sci Forum 294–296:27
47. Merkle KL, Thompson LJ (1999) Phys Rev Lett 83:556
48. Medlin DL, Foiles SM, Cohen D (2001) Acta Mater 49:3689
49. Medlin DL, Cohen D, Pond RC (2003) Philos Mag Lett 83:223
50. Westmacott KH, Hinderberger S, Dahmen U (2001) Philos Mag A 81:1547
51. Song SG, Vetrano JS, Bruemmer SM (1997) Mater Sci Eng A 232:23
52. Frank FC (1950) In: A symposium on the plastic deformation of crystalline solids. Office of naval research, Washington, DC, p 151
53. Read WT (1953) Dislocations in crystals. McGraw-Hill, New York
54. Sutton AP, Balluffi RW (1995) Interfaces in crystalline solids. Clarendon Press, Oxford